Int. J. Heat Mass Transfer. Vol. 34, No. 10, pp. 2641–2652, 1991
Printed in Great Britain

0017–9310/91 $3.00+0.00

On the frequency response of wall transfer probes

NEIMA BRAUNER
Department of Fluid Mechanics, Faculty of Engineering, Tel-Aviv University, Ramat-Aviv 69978, Israel

(*Received* 19 *December* 1989 *and in final form* 24 *September* 1990)

Abstract—The time response of wall transfer probes may significantly affect the interpretation of the physical phenomena involved. The transfer function between the heat or mass flux at the probe surface and the wall shear is analysed in the frequency domain. Space variation induced by the finite propagation velocity of a fluctuating wall shear is considered, as frequently encountered in various two-phase flow systems. The analysis indicates that the response is determined by two parameters—the non-dimensional frequency and the non-dimensional fluctuation velocity. The amplitude and phase corrections, which are to be applied to pseudosteady model calculations are numerically calculated. It is found that as the wall shear fluctuation is slowed down the probe frequency response significantly deteriorates. The sensitivity of the response to the fluctuation velocity reduces as the Prandtl or Schmidt numbers increase, indicating a superiority of electrochemical probes over themal probes.

1. INTRODUCTION

THE INFORMATION about the variation of the local and instantaneous wall shear stress is often found to be useful in analysing various single and two-phase flows. The development of small, flush mounted wall transfer probes, capable of measuring the instantaneous heat or mass transfer rates, offers the opportunity of obtaining insight on the flow characteristics in the near wall region. However, meaningful and successful interpretation of experimental data depends, in a very critical manner, on the knowledge of the dynamic behaviour or transfer function of the measuring device used.

The mass transfer probe is based upon the diffusion controlled electrolysis technique, developed by Reiss and Hanratty [1]. The surface of the probe forms an electrode which is maintained at a constant (zero) concentration and the mass transfer rate is determined by measuring the current in the electrolysis cell. With heat transfer probes, the instantaneous transfer rates at the wall are obtained by measuring the heating power required for maintaining a constant probe temperature.

Various experimental and theoretical aspects concerning the application of wall transfer probes have been reviewed by Hanratty and Campbell [2]. These probes have been used extensively in experimental studies of single phase flows, for example, the studies of turbulent wall shear fluctuation in steady and pulsating pipe flows [3–7]. In studies of two-phase flows these probes have been used to measure the average wall shear, as well as the magnitude and direction of the fluctuation induced by the wavy gas–liquid interface [8–15].

It is by now well established that a significant error can arise in interpreting data concerning a fluctuating wall shear due to the capacitance effect of the concentration or thermal boundary layers. Only for a slowly varying velocity field, can a pseudosteady state assumption be made, whereby the instantaneous mass transfer coefficient and the instantaneous velocity gradient are related by steady flow model equations. Asymptotic solution for the frequency response of the transfer rates at the wall to a *uniform* (in space) fluctuating wall shear, in the limits of high and low frequencies, have been presented by Lighthill [16] and Bellhouse and Schultz [17]. Fortuna and Hanratty [18] and later, Mao and Hanratty [19] obtained numerical results for the corrections which are to be applied to the pseudosteady state solution when a wall shear fluctuation of an arbitrary frequency is concerned. The effect of accounting for the diffusion in the axial direction on the probe frequency response was recently studied by Ambari *et al.* [20]. These studies show that the use of the pseudosteady state assumption always introduces an error in the determination of the instantaneous wall shear stress. Moreover, the larger the Schmidt or Prandtl numbers the lower the probe cut-off frequency. Hence, a detailed knowledge of the probe frequency response is essential for its meaningful application.

The above-mentioned frequency response studies [16–20] are based on the assumption of a uniform flow field, whereby no space variation in the average wall shear or in its fluctuation are allowable. Indeed, the assumption of uniform fluctuation in space does not introduce any limitation for the applicability of the analysis to pipe flow oscillations induced by pressure waves. In studies of two-phase flows, however, the wall shear oscillations are strongly related to the mobile interfacial waves. Here, space variation of the

NOMENCLATURE

A amplitude ratio, equation (21)
C non-dimensional wave celerity
F non-dimensional temperature or concentration
f fluctuating component of F
$\hat{f}$ fluctuation amplitude
$\tilde{f}$ relative fluctuation, $\hat{f}\bar{S}/\hat{s}$
g gravitational acceleration [m s^{-2}]
h film thickness [m]
K transfer coefficient [m s^{-1}]
$\bar{K}$ steady state transfer coefficient [m s^{-1}]
k fluctuating component of transfer coefficient [m s^{-1}]
$\hat{k}$ amplitude of k [m s^{-1}]
$\hat{k}_s$ amplitude of k for pseudosteady solution [m s^{-1}]
L length of transfer element [m]
L^+ non-dimensional length of transfer element, Lu^*/ν
N Schmidt number or Prandtl number, ν/α
p pressure [N m^{-2}]
Re film Reynolds number, $4\Gamma/\mu$
S velocity gradient at the wall [s^{-1}]
$\bar{S}$ time average of S [s^{-1}]
s fluctuating component of S [s^{-1}]
$\hat{s}$ amplitude of s [s^{-1}]
T temperature [°C]
t time
U non-dimensional disturbance propagation velocity, equation (14)
$\bar{u}$ average film velocity [m s^{-1}]
u axial velocity [m s^{-1}]
u^* friction velocity, $(\nu\bar{S})^{1/2}$ [m s^{-1}]
V_w perturbation propagation velocity [m s^{-1}]
v perpendicular velocity component [m s^{-1}]
W non-dimensionless frequency, $\omega^* L^{+2/3}$
X dimensionless downstream distance, equation (8)
x downstream distance [m]
Y non-dimensional distance perpendicular to the wall
y distance perpendicular to the wall [m].

Greek symbols
α diffusivity of mass or heat [m^2 s^{-1}]
Γ film flow rate [kg m^{-1} s^{-1}]
δ boundary layer thickness [m]
η similarity variable defined in equation (10)
Θ phase (lag or lead) of $\hat{k}$ relative to $\hat{s}$
λ wavelength [m]
μ viscosity [kg m^{-1} s^{-1}]
ν kinematic viscosity [m^2 s^{-1}]
τ_i film interfacial shear [N m^{-2}]
ϕ pressure drop factor, Table 1
ω angular velocity [rad s^{-1}]
ω^* dimensionless angular velocity, equation (14)
ω^+ dimensionless angular velocity, $\omega\nu/u^{*2}$.

Subscripts
b bulk
s pseudosteady model, or sheared interface
w wall.

Superscripts
$\bar{}$ time average
$\hat{}$ fluctuation amplitude
$+$ non-dimensionalized by u^* and ν.

fluctuating wall shear may be of importance in evaluating the probe frequency response, and therefore, may affect the interpretation concerning the amplitude and phase relations between the wall shear and the passing-by interfacial wave.

It is therefore the purpose of the present study to extend the frequency response analysis of wall transfer probes to a propagating wall shear fluctuation.

2. THE GOVERNING EQUATIONS

The problem of interest is the unsteady heat or mass transfer to a two-dimensional small wall element (probe) aligned with its long side, w, perpendicular to the direction of the mean flow. The conditions at the probe surface are controlled so that it is maintained at a constant temperature, T_w (or constant concentration, C_w), which differs from that in the bulk oncoming fluid (T_b or C_b). For sufficiently wide probes ($w \gg L$), the temperature or concentration in the developing boundary layer is governed by the unsteady two-dimensional conservation equations

$$\frac{\partial u}{\partial x}+\frac{\partial v}{\partial y}=0 \tag{1}$$

$$\frac{\partial F}{\partial t}+u\frac{\partial F}{\partial x}+v\frac{\partial F}{\partial y}=\alpha\left(\frac{\partial^2 F}{\partial y^2}+\frac{\partial^2 F}{\partial x^2}\right) \tag{2}$$

where F stands for either the non-dimensional temperature $(=(T-T_w)/(T_b-T_w))$ or concentration $(=(C-C_w)/(C_b-C_w))$, α is the fluid (thermal or mass) diffusivity, y the distance from the wall and x the distance in the mean flow direction, as schematically described in Fig. 1. The relevant boundary conditions are

$$F(\pm\infty, y, t)=F(x,\infty,t)=1$$
$$F(x,0,t)=0;\quad 0\leqslant x\leqslant L$$
$$\frac{\partial F}{\partial y}(x,0,t)=0;\quad x<0;\quad x>L. \tag{3}$$

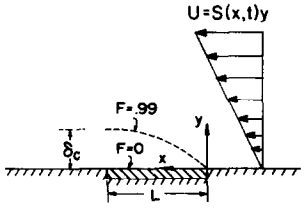

FIG. 1. Schematic description of a wall transfer probe.

If the probe length is small enough, the concentration or thermal boundary layer which develops over it will be so thin, that the velocity field is well described by

$$u = S(x,t)y; \quad v = -\frac{1}{2}\frac{\partial S}{\partial x}y^2 \tag{4}$$

where S is the velocity gradient at the wall. The velocity gradient at the wall and the resulting temperature (or concentration) are expressed as a sum of steady and fluctuating terms

$$S(x,t) = \bar{S}(x)+s(x,t); \quad F(x,t) = \bar{F}(x)+f(x,t). \tag{5}$$

Note that the perpendicular velocity v, which has been ignored in previous studies [18, 19], is retained here, since spacial variation of the wall shear is to be considered, $s = s(x,t)$. For a steady uniform flow field $\bar{S} = \text{const.}$, and the substitution of equation (5) into equations (2)–(4) yields for the steady field, $\bar{F}$

$$\bar{S}y\frac{\partial \bar{F}}{\partial x} = \alpha\left(\frac{\partial^2 \bar{F}}{\partial y^2}+\frac{\partial^2 \bar{F}}{\partial x^2}\right) \tag{6}$$

$$\bar{F}(x,\infty) = \bar{F}(\pm\infty, y) = 1 \tag{6a}$$

$$\bar{F}(x,0) = 0; \quad 0 \leqslant x < L \tag{6b}$$

$$\frac{\partial \bar{F}}{\partial y}(x,0) = 0; \quad x < 0; \quad x > L \tag{6c}$$

and for the fluctuation term, f

$$\frac{\partial f}{\partial t}+(\bar{S}+s)y\frac{\partial f}{\partial x}-\frac{1}{2}y^2\frac{\partial s}{\partial x}\frac{\partial f}{\partial y}-\alpha\left(\frac{\partial^2 f}{\partial y^2}+\frac{\partial^2 f}{\partial x^2}\right) = \frac{1}{2}y^2\frac{\partial s}{\partial x}\frac{\partial \bar{F}}{\partial y}-sy\frac{\partial \bar{F}}{\partial x} \tag{7}$$

$$f(\pm\infty, y, t) = f(x,\infty,t) = 0 \tag{7a}$$

$$f(x,0,t) = 0; \quad 0 \leqslant x \leqslant L \tag{7b}$$

$$\frac{\partial f}{\partial y}(x,0,t) = 0; \quad x < 0; \quad x > l. \tag{7c}$$

In terms of the non-dimensional variables

$$X = x/L = x^+/L^+; \quad L^+ = \frac{Lu^*}{\nu}; \quad u^* = (\nu\bar{S})^{1/2}$$

$$Y = y^+\left(\frac{N}{L^+}\right)^{1/3}; \quad y^+ = \frac{yu^*}{\nu}; \quad N = \nu/\alpha \tag{8}$$

equation (6) reads

$$Y\frac{\partial \bar{F}}{\partial X} = \frac{\partial^2 \bar{F}}{\partial Y^2}+\frac{1}{N^{2/3}L^{+4/3}}\frac{\partial^2 \bar{F}}{\partial X^2}. \tag{9}$$

Note that N is either the Schmidt number or the Prandtl number. For $N^{2/3}L^{+4/3} \gg 1$ the diffusion in the main flow direction may be neglected, and the (steady state) solution of equation (9) reads [1]

$$\bar{F} = \frac{1}{\Gamma(4/3)}\int_0^\eta e^{-z^3}\,dz; \quad \eta = Y/(9X)^{1/3}. \tag{10}$$

The fluctuating term, f, is to be obtained by solving equation (7) for a specified fluctuating velocity gradient, s. If a progressive harmonic disturbance in the flow field is considered, its time and space variations are specified by

$$s = \hat{s}e^{-i(2\pi/\lambda)(x-V_w t)} = \hat{s}e^{i\omega t}e^{-i\omega x/V_w}; \quad \omega = \frac{2\pi}{\lambda/V_w} \tag{11}$$

where $\hat{s}$ is the (real) disturbance amplitude of frequency ω, progressing downstream at a velocity V_w. For $\hat{s}/\bar{S} \ll 1$ the linearized form of equations (7) may be considered, in which the solution for f takes the form

$$f = \hat{f}_1(x,y)e^{i\omega t} = \hat{f}(x,y)e^{-i\omega x/V_w}e^{i\omega t}. \tag{12}$$

Note that $\hat{f}$ is generally a complex number. Substituting equations (11) and (12) into equations (7) the following non-dimensional equation for $\tilde{f} = \hat{f}\bar{S}/\hat{s}$ is obtained:

$$iW[1-UY]\tilde{f}+Y\frac{\partial \tilde{F}}{\partial X}-\frac{\partial^2 \tilde{f}}{\partial Y^2}-\frac{1}{N^{2/3}L^{+4/3}}\left[\frac{\partial^2 \tilde{f}}{\partial X^2}-W^2U^2\tilde{f}\right] = -i\frac{WU}{2}Y^2\frac{\partial \bar{F}}{\partial Y}-Y\frac{\partial \bar{F}}{\partial X} \tag{13}$$

with

$$\tilde{f} = \hat{f}\bar{S}/\hat{s}; \quad W = \omega^* L^{+2/3}; \quad \omega^* = \frac{\omega\nu}{u^{*2}}N^{1/3};$$

$$U = \frac{u^*}{V_w}\left(\frac{L^+}{N}\right)^{1/3}. \tag{14}$$

Again, for sufficiently large $N^{2/3}L^{+4/3}$ the fourth term on the left-hand side of equation (13), which evolves from retaining the diffusion in the downstream direction, may be ignored. Substituting the steady solution for $\bar{F}$ (equation (10)) in equation (13) yields

$$iW[1-UY]\tilde{f}+Y\frac{\partial \tilde{f}}{\partial X}-\frac{\partial^2 \tilde{f}}{\partial Y^2} = \frac{1}{0.893}\frac{Y^2}{(9X)^{1/3}}e^{-Y^3/9X}\left[-i\frac{WU}{2}+\frac{1}{3X}\right] \tag{15}$$

with

$$\tilde{f}(X,0)=0;\quad 0\leqslant X\leqslant 1$$
$$\tilde{f}(0,Y)=0;\quad \tilde{f}(X,\infty)=0. \tag{15a}$$

It is to be noted that the case of uniform fluctuating velocity field, whereby $s\neq s(x)$, is obtained in the limit of $V_w\to\infty$ or $U\to 0$. In this case the formulation reduces to that presented by Fortuna and Hanratty [18] and Mao and Hanratty [19].

2.1. *The transfer coefficient*

The measurable quantity is the instantaneous heat or mass transfer rate averaged over the wall element. The corresponding space average transfer coefficient is defined by

$$K=\frac{\alpha}{L}\int_0^L \left.\frac{\partial F}{\partial y}\right|_{y=0}\mathrm{d}x. \tag{16}$$

Note that K stands for either the average mass transfer coefficient or the heat transfer coefficient divided by ρc_p. At steady state conditions ($F=\bar{F}$), the corresponding $\bar{K}$ is obtained by substituting equations (10) into equation (16), whereby

$$\overline{Sh}=\frac{\bar{K}L}{\alpha}=0.807L^{+2/3}N^{1/3};$$
$$\bar{K}=0.807\left(\frac{\alpha^2\bar{S}}{L}\right)^{1/3}. \tag{17}$$

At unsteady conditions the instantaneous transfer coefficient is represented as a sum of an average (steady) and fluctuating term and is derived by substituting equations (5) and (12) into equation (16)

$$K=\bar{K}+k=\bar{K}+\frac{\alpha}{L}\mathrm{e}^{\mathrm{i}\omega t}\int_0^L \left.\frac{\partial\hat{f}}{\partial y}\right|_{y=0}\mathrm{e}^{-\mathrm{i}\omega x/V_w}\,\mathrm{d}x$$
$$=\bar{K}+\hat{k}\,\mathrm{e}^{\mathrm{i}\omega t} \tag{18}$$

where

$$\left.\frac{\partial\hat{f}}{\partial y}\right|_{y=0}=\frac{\hat{s}}{\bar{S}}\left.\frac{\partial\bar{f}}{\partial y}\right|_{y=0}. \tag{18a}$$

Equation (18) defines the (complex) transfer coefficient amplitude, $\hat{k}$. In the limit of $\omega\to 0$, however, a quasi-steady situation may be assumed, whereby the relation obtained between the velocity gradient at the wall and the average measured transfer coefficient is defined by equation (17). For the case where the pseudosteady state assumption is valid, equation (17) yields

$$\hat{k}_s=\hat{k}(\omega\to 0)=\frac{0.807}{3}\left(\frac{\alpha^2}{L\bar{S}^2}\right)^{1/3}\hat{s}=\frac{1}{3}\frac{\hat{s}}{\bar{S}}\bar{K}. \tag{19}$$

The ratio between the *actual* amplitude of the transfer coefficient fluctuation (at arbitrary frequency, ω) and that obtained by assuming a pseudosteady situation follows from equations (8), (18) and (19)

$$\frac{\hat{k}}{\hat{k}_s}=3.717\int_0^1\left(\frac{\partial\tilde{f}}{\partial Y}\right)_{Y=0}\mathrm{e}^{-\mathrm{i}WUX}\,\mathrm{d}X$$
$$=\tilde{k}(W,U)=\tilde{k}_r+\mathrm{i}\tilde{k}_i. \tag{20}$$

The corresponding amplitude ratio and the phase angle are obtained by

$$A=|\tilde{k}|=(\tilde{k}_r^2+\tilde{k}_i^2)^{1/2};\quad \Theta=\tan^{-1}(\tilde{k}_i/\tilde{k}_r). \tag{21}$$

Equations (19)–(21) define the frequency domain transfer function between a fluctuating wall shear stress propagating downstream at a finite velocity, and the resulting (measured) transfer coefficient. The solution depends on the two non-dimensional parameters, W and U. The first represents the fluctuation frequency and the latter its relative propagation velocity. The value $A^{-1}=\hat{k}_s/|\hat{k}|$ represents the amplitude correction that must be applied at a specified frequency, if pseudosteady state relations, equations (17) and (19), are used to calculate $s(x,t)$ from the (time varying) probe signal. The value of Θ represents the phase relation between fluctuating wall shear and the resulting fluctuating transfer coefficient. Note that a negative Θ means that the measured coefficient lags the shear stress variation.

The values of $A(W,U)$ and $\Theta(W,U)$ are obtained by solving numerically equation (15) for $\tilde{f}$ and then carrying out the integration in equation (20). Equation (15) is solved by applying the Crank–Nicholson six-point implicit method. The tridiagonal equations system obtained is solved by means of the standard double sweep Thoma's algorithm.

The numerical results are presented in Section 4. Asymptotic analytic solutions obtained in the limit of low and high frequencies are presented first in Section 3.

3. ASYMPTOTIC SOLUTIONS

In the limit of low frequencies, where the quasi-steady state assumption is valid, the instantaneous fluctuation in the concentration (or temperature) field, f, and that of the velocity gradient are in phase. The differential equation for $\hat{f}_s=\hat{f}(\omega\to 0)$ is obtained by substituting $F=\bar{F}+\hat{f}_s$, $S=\bar{S}+\hat{s}$ in equation (6) ($(NL^{+2})\gg 1$ is assumed). For $\hat{f}_s/\bar{F},\hat{s}/\bar{S}\ll 1$ only linear terms are retained, whereby

$$Y\left[\frac{\partial\tilde{f}_s}{\partial X}+\frac{\partial\bar{F}}{\partial X}\right]=\frac{\partial^2\tilde{f}_s}{\partial Y^2};\quad \tilde{f}_s=\hat{f}_s\bar{S}/\hat{s}. \tag{22}$$

The solution for $\hat{f}_s$ may thus be derived from the solution for F at steady state (equation (10))

$$\hat{f}_s=\hat{s}\left.\frac{\partial F}{\partial S}\right|_{S=\bar{S}}=\hat{s}\left[\frac{\partial F}{\partial\eta}\frac{\partial\eta}{\partial S}\right]_{S=\bar{S}}=\frac{1}{3}\frac{\hat{s}}{\bar{S}}Y\frac{\partial\bar{F}}{\partial Y}. \tag{23}$$

The corresponding fluctuation of the transfer coefficient $\hat{k}_s$ is obtained by equation (19), and is also in phase with the velocity gradient fluctuation. However, with increasing frequency, these are no longer in

phase. The phase change in the low frequency region, $W \ll 1$, may be estimated following the analysis outlined by Lighthill [16] and Fortuna and Hanratty [18]. Assume

$$\tilde{f} = f_s + iW\tilde{f}_1; \quad W = \omega^* L^{+2/3}. \tag{24}$$

Substitution of equation (24) in equation (15) and retaining terms of the order of W^1 yields

$$[1-UY]\tilde{f}_s + Y\frac{\partial \tilde{f}_1}{\partial X} = \frac{\partial^2 \tilde{f}_1}{\partial Y^2} - \tfrac{1}{2}UY^2\frac{\partial \bar{F}}{\partial Y}. \tag{25}$$

An approximate solution for $\tilde{f}_1$ can be obtained by using an integral approach. Equation (25) is integrated over the perpendicular direction

$$\int_0^\infty [1-UY]\tilde{f}_s\,dY + \frac{d}{dx}\int_0^\infty Y\tilde{f}_1\,dY + \tfrac{1}{2}U\int_0^\infty Y^2\frac{\partial \bar{F}}{\partial Y} = -\left.\frac{\partial \tilde{f}_1}{\partial Y}\right|_{Y=0}. \tag{26}$$

The variation of $\tilde{f}_1$ in the perpendicular direction is chosen so as to satisfy the conditions that $\tilde{f}_1$ and $\partial^2\tilde{f}_1/\partial Y^2$ are zero at the wall and $\tilde{f}_1$, $\partial\tilde{f}_1/\partial Y$, $\partial^2\tilde{f}_1/\partial Y^2$ vanish as $Y \to \infty$. The following relation satisfies the above conditions:

$$\tilde{f}_1 = B(X)Y\frac{\partial \bar{F}}{\partial Y}. \tag{27}$$

Substituting equations (10), (23) and (27) into equation (26), integrating and equating terms to the equal power of X yields

$$\tilde{f} = \tfrac{1}{3}Y\frac{\partial \bar{F}}{\partial Y}[1-i(B_1X^{2/3}+B_2UX)W];$$

$$B_1 = 0.55; \quad B_2 = \tfrac{1}{4}. \tag{28}$$

The constants B_1 and B_2 have been checked against the results obtained by numerical solution of equation (15) in the limit of low frequencies.

The corresponding amplitude and phase corrections, which are to be applied to the transfer coefficient calculated by assuming pseudosteady state, are derived by substituting equation (28) in equation (20) and retaining terms linear in W. In the low frequency limit, the equivalent of equation (20) reads

$$\frac{\hat{k}}{\hat{k}_s} = 1 - \tfrac{1}{2}iW[0.55+U] \tag{29}$$

whereby

$$\Theta = -\tan^{-1}\{\tfrac{1}{2}W[0.55+U]\} \simeq -\tfrac{1}{2}W[0.55+U]. \tag{30}$$

Equation (30) indicates that in the low frequency range, and for $U \geqslant 0$, the instantaneous transfer coefficient lags the fluctuating wall shear. The phase lag increases linearly with W (either increasing frequency or probe length). Slowing down a streamwise propagating wall shear fluctuation (increasing U) affects higher phase lag. However, with a counter-current propagating disturbance ($U < 0$), lower phase lag is to be expected, or even a phase lead (for $U < -0.55$). The amplitude ratio decreases with W, and its sensitivity to frequency of oscillations increases with U. In the limit of $W \ll 1$ the amplitude correction factor is found to obey

$$\frac{1}{A^2} = \left|\frac{\hat{k}_s}{\hat{k}}\right|^2 = 1 + [0.056 + 0.084U^2 + 0.004U]W^2. \tag{31}$$

In the high frequency range, $W \gg 1$, the term $Y\,\partial\tilde{f}/\partial x$ in equation (15) may be neglected [16]. If in addition $UY \ll 1$ is assumed, equation (15) can be integrated to yield

$$\tilde{f} = \frac{2}{3(9)^{1/3}\Gamma(4/3)}[\exp(-\sqrt{(iW)}Y) - 1 - \tfrac{1}{2}WY^2] \times \frac{(1-\frac{3}{2}iWUX)}{W^2X^{4/3}} \tag{32}$$

whereby

$$\left.\frac{\partial \tilde{f}}{\partial Y}\right|_{Y=0} = -\frac{2\sqrt{i}}{3(9)^{1/3}\Gamma(4/3)}\frac{(1-\frac{3}{2}iWUX)}{W^{3/2}X^{4/3}}. \tag{33}$$

Substituting equation (33) into equation (20) and integrating yields

$$\left.\frac{\hat{k}}{\hat{k}_s}\right|_{W\to\infty} = \left.\frac{\hat{k}}{\hat{k}_s}\right|_{(W\to\infty, U=0)} + 3\frac{U}{W^{1/2}}i^{3/2} \tag{34}$$

where

$$\left.\frac{\hat{k}}{\hat{k}_s}\right|_{W\to 0, U=0} = -\tfrac{4}{3}\frac{\sqrt{i}}{W^{3/2}}\int_0^1 \frac{1}{X^{4/3}}\,dX. \tag{35}$$

The integral in equation (35) diverges, as noticed by Ambari *et al.* [20]. This divergency probably evolves from the thinning of the Stokes layer thickness, $\delta_s = \sqrt{(2\nu/\omega)}$, to values which are of the order of the diffusion boundary layer thickness, δ_c. The Stokes layer thickness represents the region where the magnitude of the velocity oscillation changes significantly. Consequently, the assumption of a linear variation of velocity within the diffusion boundary layer is restricted to finite oscillation frequency, whereby $\delta_c \ll \delta_s$ corresponding to $W < 0.11N^{3/2}$. Moreover, for $U \neq 0$, the value of UW is to be bounded in order to justify the neglection of the term $(UW)^2\tilde{f}$ in equation (13) (which evolves from the axial diffusion term). Accordingly, the solution of equation (15) is to be limited to finite oscillation frequencies, W, in the range where the integration of equation (35) does not diverge and $(UW)^2/(NL^{+2})^{2/3} \ll 1$.

A curve fit to a power-law is performed on the numerical calculated values of $\partial\tilde{f}/\partial Y$ at the wall near the probe leading edge ($\partial\tilde{f}/\partial Y|_{Y=0} = aX^n$). When the exponent n turns out to be less than -1, the integral in equation (20) diverges. The values obtained for the exponent are presented in Fig. 2 as a function of frequency. It is shown that for low U the exponent n

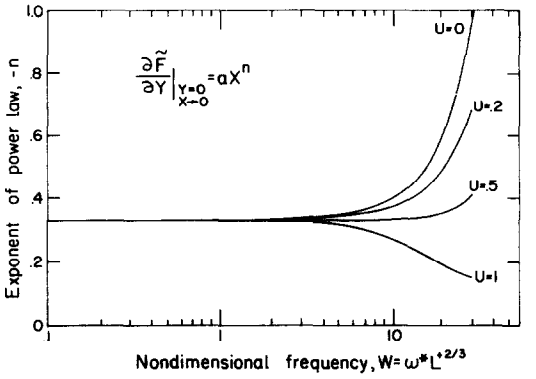

FIG. 2. Variation of the gradient at the wall near the probe leading edge.

decreases as the frequency increases, and there exists a critical frequency for which n indeed approaches -1. For instance for $U = 0$, $n \to -1$ for $W \simeq 30$, indicating that the analysis cannot be carried out beyond this frequency. For $U \neq 0$, though higher frequencies still yield convergence, the neglection of the axial diffusion must be justified (see equation (13)). Hence

$$W \ll (NL^{+2})^{1/3}/|U| = \left|\frac{V_w}{u^*}\right| L^{+1/3} N^{2/3} \qquad (36)$$

must be maintained.

4. DISCUSSION

The non-dimensional mathematical formulation indicates that the frequency response of the (measured) instantaneous transfer rate to a fluctuating wall shear is determined by two parameters: the non-dimensional fluctuation frequency $W = \omega^* L^{+2/3}$ and the propagation velocity represented by $U = (u^*/V_w)(L^+/N)^{1/3}$. The frequency response is represented by the amplitude of the transfer function k/s (normalized by its value when the frequency tends to zero) and the corresponding phase lag. These correspond to A and Θ defined in equation (21).

Figure 3 presents plots of $1/A^2$ and Θ as functions of W obtained for $U = 0$. This case corresponds to a fluctuating wall shear which propagates at an infinite

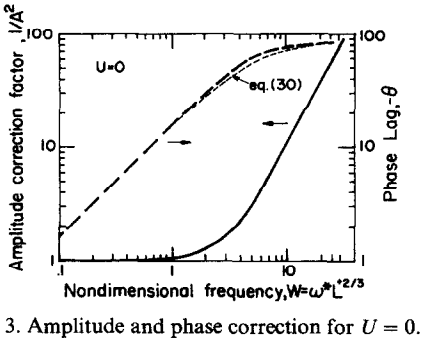

FIG. 3. Amplitude and phase correction for $U = 0$.

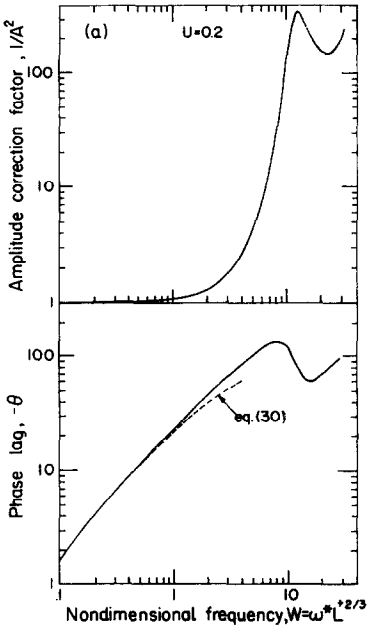

FIG. 4. Amplitude and phase corrections for $U = 0.2$.

velocity, as in the pulsating pipe flow of an incompressible fluid, whereby a uniform (in space) fluctuating wall shear is induced. As noted earlier, with $U = 0$ the formulation reduces to that presented by Fortuna and Hanratty [18] and Mao and Hanratty [19]. Indeed, the results presented in Fig. 3 are identical to those obtained by Mao and Hanratty. The value of $1/A^2$ stands for the correction factor to be applied to the power spectrum density of the wall shear obtained via pseudosteady state model calculations. For $U = 0$ the amplitude correction factor and the corresponding phase lag are found to increase monotonously with the non-dimensional frequency parameter, W.

Plots of the amplitude correction factor and phase lag obtained for $U > 0$ are presented in Figs. 4–6. Higher values of U correspond to slower propagating wall shear fluctuation, the velocity being scaled with reference to the shear velocity of the average flow field, u^*. Comparison of Figs. 3–6 reveals that, generally, the amplitude correction factor and the phase lag increase when the fluctuating wall shear is slowed down (increasing U). For sufficiently low frequencies, the calculated phase lag follows the analytic asymptotic solution given in equation (30). For higher frequencies, quite different trends of the amplitude ratio and phase lag are noticed for $U = 0$ and $U \neq 0$. Recalling that whenever the probe length, L, equals the wavelength $\lambda = 2\pi V_w/\omega$ (or integer multiples of the wavelength, $L = m\lambda$) the wall shear fluctuation is averaged-out over the probe surface, an oscillatory behaviour is to be expected in the frequency response. In terms of the non-dimensional parameters W, U the wavelength equals the probe length when $WU = 2\pi$. Inspection of Figs. 4–6 reveals that, indeed, the ampli-

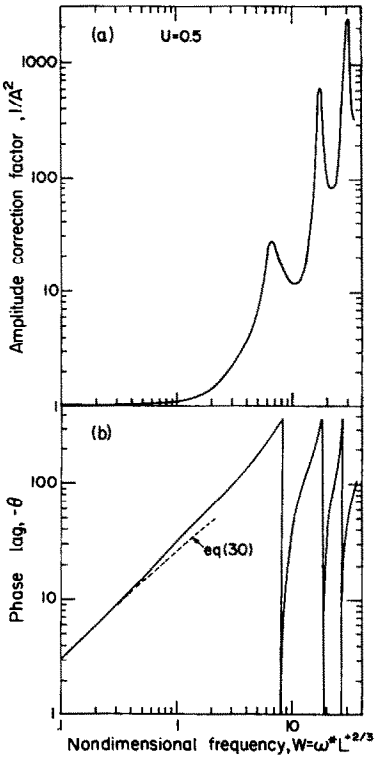

FIG. 5. Amplitude and phase corrections for $U = 0.5$.

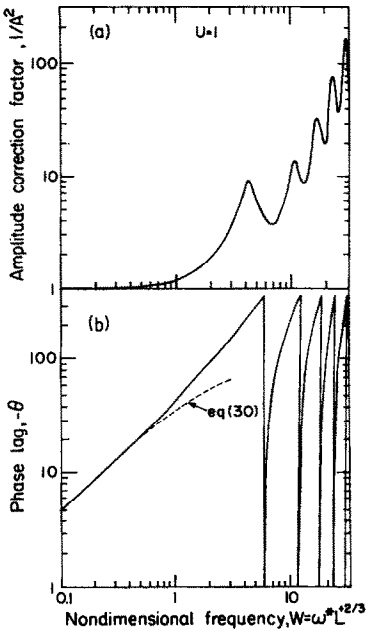

FIG. 6. Amplitude and phase corrections for $U = 1$.

tude correction factor increases dramatically whenever $W = 2\pi/U$ is approached. Thereafter (for higher W) an oscillatory variation with W is established. The corresponding phase lag, Θ, may exceed 2π, whereby the phase information between the wall shear fluctuation and measured fluctuating transfer rate is practically lost. Therefore, the frequency range where meaningful information on the wall shear fluctuation may be deduced from the transfer rate measurements is practically limited to $W < 2\pi/U$. The plots of $1/A^2$ and Θ obtained in this range are summarized in Fig. 7 for a wide range of U ($0 \leqslant U \leqslant 10$).

It is of interest at this point to refer to the practical range of the parameter U. Recently, wall transfer probes have been applied in experimental systems of falling films, as well as in a variety of two-phase sheared film flows [8–15], in an attempt to find the phase and magnitude relations between the instantaneous wall shear fluctuations and the corresponding passing-by interfacial wave. Clearly, these can be deduced provided the probe frequency response as a function of U and W is known and properly accounted for. The expected range of the parameter U in wavy film flow has been evaluated in ref. [23] and the results are summarized in Table 1.

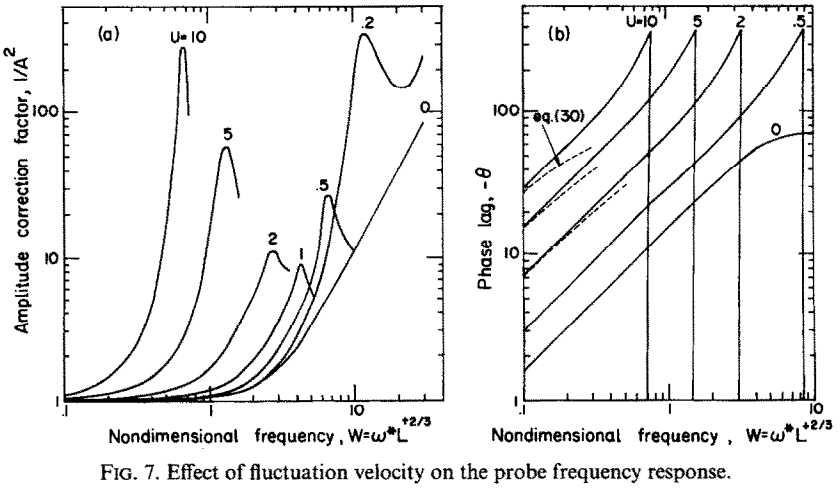

FIG. 7. Effect of fluctuation velocity on the probe frequency response.

Table 1. Evaluation of U in wavy film flow

	Laminar Nusselt's film	Turbulent falling film [21]	Sheared laminar film [22]
$h=$	$\left(\frac{3}{4}\frac{\nu^2 Re}{g}\right)^{1/3}$; $Re=4\Gamma/\mu$	$0.135\left(\frac{\nu^2}{g}\right)^{1/3} Re^{7/12}$	$\left[\frac{3}{4}\frac{\nu^2 Re}{g\phi}\right]^{1/3}\left(1+\frac{3}{2}\tilde{\tau}_i\right)^{-1/3}$ $\tilde{\tau}_i=\frac{\tau_i}{\rho\phi g h_s}$; $\phi=1+(-\partial p_g/\partial x)/\rho g$
$u^*=$	$(\nu\bar{S})^{1/2}=(gh)^{1/2}$	$0.367(\nu g)^{1/3} Re^{7/24}$	$[g\phi h(1+\tilde{\tau}_i)]^{1/2}$
$u^*/V_w=$	$\frac{3.42}{C Re^{1/2}}$	$\frac{1.335}{C Re^{1/24}}$	$\frac{3.42}{C Re^{1/2}}\left\lvert\frac{1+\tilde{\tau}_i}{1+1.5\tilde{\tau}_i}\right\rvert^{1/2}\operatorname{sign}\left(\frac{1+\tilde{\tau}_i}{1+1.5\tilde{\tau}_i}\right)$
$L^+=\frac{L^* u}{\nu}=$	$0.95 Re^{1/6}\frac{L}{(\nu^2/g)^{1/3}}$	$0.37 Re^{7/24}\frac{L}{(\nu^2/g)^{1/3}}$	$0.95 Re^{1/6}\frac{L}{(\nu^2/g)^{1/3}}\frac{(1+\tilde{\tau}_i)^{1/2}}{(1+1.5\tilde{\tau}_i)^{1/6}}\phi^{1/3}$

$\tilde{\tau}_i>0$, cocurrent downflow; $-\frac{2}{3}\leqslant\tilde{\tau}_i<0$, countercurrent downflow; $\tilde{\tau}_i\leqslant-\frac{2}{3}$, cocurrent upflow ($g<0$).

According to Table 1 the value of U for a free falling film can be estimated by

$$U=\frac{u^*}{V_w}\left(\frac{L^+}{N}\right)^{1/3}=\begin{cases}\dfrac{3.4}{C}\left[\dfrac{L}{(\nu^2/g)^{1/3}N}\right]^{1/3} Re^{-4/9}; \\ \text{laminar film} \\ \dfrac{1}{C}\left[\dfrac{L}{(\nu^2/g)^{1/3}N}\right]^{1/3} Re^{1/18}; \\ \text{turbulent film}\end{cases} \tag{37}$$

where Re is the film Reynolds number, $Re=4\Gamma/\mu$, and C the dimensionless wave celerity scaled with reference to the average film velocity. (For a laminar film and $Re\simeq 100$, $C\simeq 3$ and it decreases with Re. For $Re>10^3$ and a turbulent film $C\simeq 1$ [22].)

Equation (37) indicates that for a laminar free falling film the value of U decreases with increasing the film Reynolds number. For sufficiently small probes ($L\simeq 1$ mm) and $Re>100$, U is not expected to exceed the value of 0.25 even with thermal probes ($N=5$). For mass transfer probes with $N\simeq 10^3$, smaller values for U are predicted ($U<0.05$), in which case the probe frequency response for $U\neq 0$ is expected to approximately follow that obtained for $U=0$. For turbulent falling films, however, the value of U is predicted to increase with the film Reynolds number. For instance, with $L=1$ mm, $Re=10^4$, $C=1$ and water film ($\nu=0.01$ cm^2 s^{-1}), $U=2.7$ is obtained for a thermal probe ($N=5$) and $U=0.5$ for an electrochemical probe ($N\simeq 10^3$). Accordingly, the probe frequency response demonstrated in Figs. 5 and 6 may be relevant in these cases.

For sheared film flow, the value of U depends also on the interfacial shear magnitude and direction (see Table 1). For film downflow, applying a cocurrent interfacial shear, $\tilde{\tau}_i>0$, affects lower values of u^*/V_w compared to those obtained for a free falling film at the same Reynolds number. However, with a countercurrent interfacial shear, $\tau_i<0$, u^*/V_w (and U) may increase dramatically, mainly due to the decrease of the wave celerity. Indeed, stability analysis of sheared film flow [22] indicates that for $\tilde{\tau}_i\leqslant-0.5$ the most amplified waves are standing waves, whereby $C=0$, and thus u^*/V_w may attain very high values. For higher countercurrent interfacial shear ($\tilde{\tau}_i<-0.5$) the most amplified waves correspond to upward travelling waves ($C<0$), for which u^*/V_w (and U) attains high negative values. Increasing the counter shear beyond $\tilde{\tau}_i=-2/3$ results in upward film flow, whereby both the film flow and the interfacial waves travel upward and thus $C>0$ again. However, for $-2/3<\tilde{\tau}_i<-1$, $u^*<0$, and therefore negative values of u^*/V_w are predicted. With $\tilde{\tau}_i<-1$, u^*/V_w again attains positive values corresponding to cocurrent upward film flow.

Figure 7 shows the amplitude correction factor and the corresponding phase lag obtained for a wide range of U. For each value of U the relevant frequency range W is restricted to that beyond which either the phase information is lost (Θ exceeds 2π) or the amplitude correction factor starts oscillating. Evidently, with increasing U the probe frequency response significantly deteriorates, and the frequency range where a meaningful interpretation of measurements is feasible diminishes.

The effect of $U<0$ on the probe frequency response for a wide range of W is demonstrated in Figs. 8–10. It is shown that except for very low negative U, the amplitude correction factor increases with increasing $|U|$ over the entire frequency range. Again, beyond $W\simeq 2\pi/|U|$ both the amplitude correction and the phase start oscillating. For sufficiently low frequencies the numerical results obtained $1/A^2$ and Θ follows the analytic asymptotic expressions derived for $W\to 0$ (equations (30) and (31)). Indeed, the phase lag is found to decrease when compared to that predicted

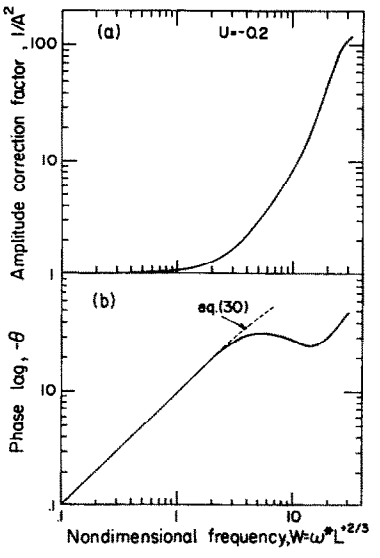

FIG. 8. Amplitude and phase corrections for $U = -0.2$.

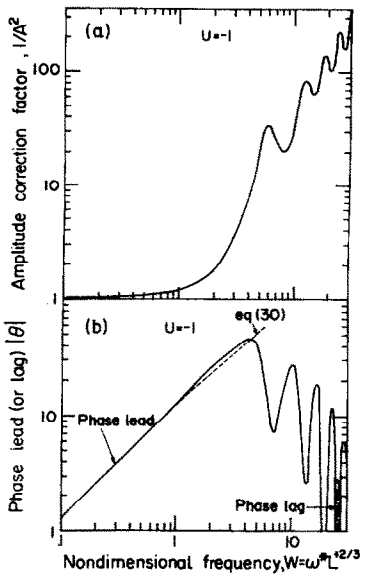

FIG. 10. Amplitude and phase corrections for $U = -1$.

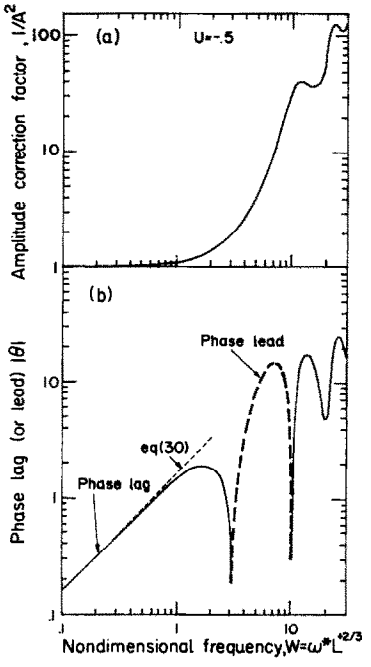

FIG. 9. Amplitude and phase corrections for $U = -0.5$.

for $U = 0$ and for $U < -0.55$ a phase lead is obtained in the low frequency range. Note that for $U = -0.5$ (Fig. 9(b)), although the low frequency range still yields a phase lag, a phase lead is predicted for higher frequencies ($3 < W < 10$).

The numerical results for the amplitude correction factor and the phase (lead) obtained for a wide range of negative U are shown in Fig. 11. As with positive U, the range of frequencies for which the pseudo-steady assumption may be expected to be valid is shown to be significantly restricted with increasing $|U|$.

5. CONCLUDING REMARKS

Wall transfer probes may be used for measuring wall shear fluctuations provided that their time response is known. The probe frequency response is shown here to depend on the two non-dimensional parameters, $W = \omega^* L^{+2/3}$ and $U = (u^*/V_w)(L^+/N)^{1/3}$. For spacial uniform wall shear fluctuation, $V_w \to \infty$ and $U = 0$, the frequency response previously predicted by Fortuna and Hanratty [18] and Mao and Hanratty [19] is recovered. In this case the probe cut-off frequency is found to decrease with increasing N (Prandtl or Schmidt numbers), apparently indicating an advantage of thermal probes over electrochemical probes. However, as has been already discussed by Mao and Hanratty [19], when the restriction which evolves from the neglection of the diffusion in the axial direction is accounted for ($L^+ \gg N^{-1/2}$), larger L^+ is required for smaller N, and consequently mass transfer probes tend to be superior to thermal probes.

The effect of a finite propagation velocity of the wall shear fluctuation on the probe frequency response is demonstrated for a wide range of U. Positive U corresponds to a fluctuation which propagates in the main flow direction, while $U < 0$ stands for situations where the wall shear fluctuation propagates countercurrently to the main flow. It is shown that with increasing $|U|$ the probe frequency response significantly deteriorates. Moreover, the possibility of extracting meaningful information of the wall shear fluctuation (while accounting for the probe time response) is restricted to $W < 2\pi/U$. Since $U \propto N^{1/3}$ it is advantageous to employ experimental setting of larger N, reinforcing the superiority of mass transfer probes over thermal probes.

This is further elucidated with reference to Fig. 12.

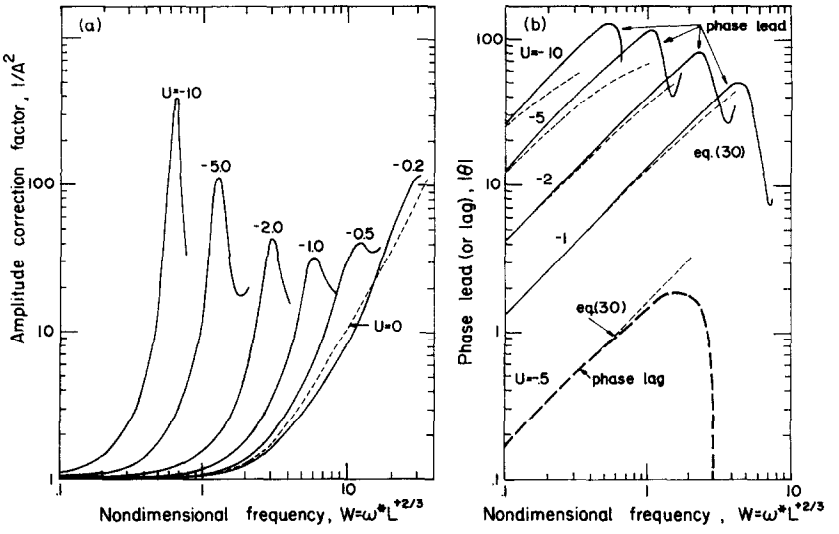

FIG. 11. Countercurrent wall shear fluctuation—effect of propagation velocity on the probe frequency response.

If we consider, for example, an electrochemical probe with $N = 10^3$, the minimum probe length for which the neglection of axial diffusion may be justified is $L^+_{\min} = 14N^{-1/2} = 0.44$ [2]. The corresponding minimum thermal probe length ($N = 5$) is $L^+_{\min} = 6.26$. Since $N^{1/3}L^{+2/3}$ is identical for the two probes ($N^{1/3}L^{+2/3} = 14^{2/3}$) the cut-off frequency ω^+ for a specified $U = (u^*/V_w)(L^+/N)^{1/3}$ is the same. However, as $(L^+/N)^{1/3}$ is significantly larger for the thermal probe the cut-off frequency at a specified u^*/V_w is expected to be larger for the electrochemical probe. Figure 12 compares the maximum frequency allowed with these two probes if corrections greater than 5% on the amplitude are to be avoided ($1/A^2 \leqslant 1.05$) as a function of u^*/V_w. It is shown that while for $u^*/V_w = 0$ the restriction on ω^+ is the same for the two probes, for $u^*/V_w \neq 0$ the cut-off frequency of the electrochemical probe is larger, indicating a superiority of the mass transfer probe over the thermal probe when larger $|u^*/V_w|$ are expected. The cut-off frequency corresponding to a phase error less than 5° is also indicated on Fig. 12. This criterion is generally found to be more restrictive than the above amplitude criterion, except in the vicinity of negative u^*/V_w corresponding to $U \sim -0.5$, where relatively large frequencies may be dictated with minor phase shifts (see also Fig. 9 and equation (30)). The electrochemical probe is shown to be superior to the thermal probe also from the viewpoint of phase correction restrictions.

It is further to be noted that $\omega^+ > 0.2$ is to be avoided with the thermal probe if the Stokes layer restriction ($W < 0.11N^{3/2}$) is considered, while for the

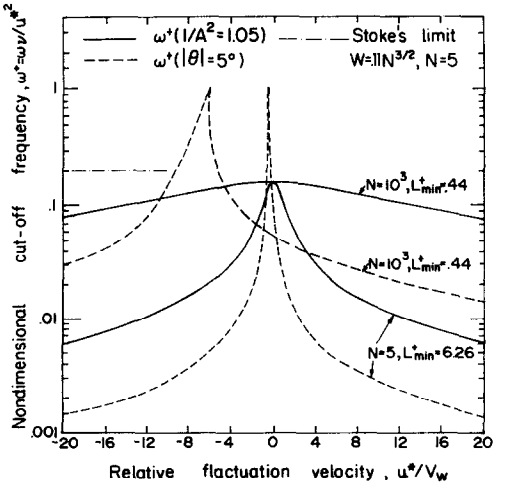

FIG. 12. Cut-off frequency—comparison between thermal and electrochemical probes.

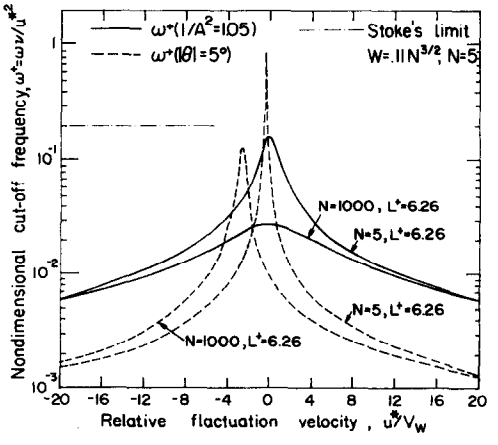

FIG. 13. Cut-off frequency for thermal and electrochemical probes of equal size.

electrochemical probe this restriction does not impose any practical limitation ($\omega^+ < 600$ for $N = 10^3$, $L^+ = 0.44$).

Complementary to Fig. 12, Fig. 13 compares the above cut-off frequencies (for $1/A^2 < 1.05$ or $|\Theta| < 5°$) when the electrochemical probe length is increased to $L^+ = 6.26$. It is concluded that the advantage of the thermal probe over an equal size electrochemical probe is limited to low u^*/V_w and diminishes as u^*/V_w increases. For $u^*/V_w < -2$ the phase correction cut-off frequency is shown to be larger for the electrochemical probe.

Finally, it is to be noted that in practical situations non-linear effects may be of importance and therefore in utilizing the above (linear) results, nonlinearities ought to be considered.

REFERENCES

1. L. P. Reiss and T. J. Hanratty, An experimental study of the unsteady nature of the viscous sublayer, *A.I.Ch.E. Jl* **9**, 154 (1963).
2. T. J. Hanratty and J. A. Campbell, Measurement of wall shear stress. In *Fluid Mechanics Measurements* (Edited by R. J. Goldstein). Hemisphere, Washington, DC (1983).
3. J. E. Mitchell and T. J. Hanratty, A study of turbulence at wall using an electrochemical wall shear stress meter, *J. Fluid Mech.* **26**, 199 (1966).
4. T. Mizushina, T. Maruyama, S. Ide and Y. Mizukami, Dynamic behavior of transfer coefficient in pulsating laminar tube flow, *J. Chem. Engng Jap.* **6**, 152 (1973).
5. B. R. Ramaprian and S. W. Tu, Fully developed periodic turbulent pipe flow. Part 2. The detailed structure of the flow, *J. Fluid Mech.* **137**, 59 (1983).
6. Z. X. Mao and T. J. Hanratty, Studies of the wall shear stress in a turbulent pulsating pipe flow, Ph.D. Thesis, University of Illinois, Urbana (1984).
7. P. Zilker and T. J. Hanratty, Influence of the amplitude of a solid wavy wall on a turbulent flow, Part 2. Separated flows, *J. Fluid Mech.* **90**, 257 (1979).
8. A. M. Sutey and J. G. Knudsen, Mass transfer at the solid–liquid interface for climbing film flow in an annular duct, *A.I.Ch.E. Jl* **15**, 519 (1969).
9. V. E. Nakoryakov, O. N. Kashinsky, A. P. Burdokov and V. P. Odnoral, Local characteristics of upward gas–liquid flows, *Int. J. Multiphase Flow* **7**, 63 (1981).
10. G. Cognet, M. Lebouche and M. Souhar, Wall shear measurements by electrochemical probe for gas–liquid two-phase flow in vertical duct, *A.I.Ch.E. Jl* **30**(2), 338 (1984).
11. N. Brauner and D. Moalem-Maron, Characteristics of inclined thin films waviness and the associated mass transfer, *Int. J. Heat Mass Transfer* **25**(1), 99 (1982).
12. D. Moalem-Maron, N. Brauner and A. E. Dukler, Interfacial structure of thin falling films: piecewise modelling of the waves, *Physiochem. Hydrodyn.* **6**, 87 (1985).
13. G. J. Zabaras, Studies of vertical gas liquid flows, Ph.D. Thesis, University of Houston (1985).
14. A. H. Govan, G. F. Hewitt, D. G. Owen and G. Burnett, Wall shear measurements in vertical air water annular two-phase flow, *Int. J. Multiphase Flow* **15**(3), 307 (1989).
15. Y. Hagiwara, E. Esmaeilzadeh, H. Tsutsui and K. Suzuki, Simultaneous measurement of liquid film thickness, wall shear stress and gas flow turbulence of horizontal wavy two phase flow, *Int. J. Multiphase Flow* **15**(3), 421 (1989).
16. M. J. Lighthill, The response of laminar skin friction and heat transfer to fluctuations in the stream velocity, *Proc. R. Soc.* **224A**, 1 (1954).
17. B. J. Bellhouse and D. L. Schultz, The measurement of fluctuating skin friction in air with heated thin-film gauges, *J. Fluid Mech.* **32**, 675 (1968).
18. G. Fortuna and T. J. Hanratty, Frequency response of the boundary layer on wall transfer probes, *Int. J. Heat Mass Transfer* **14**, 1499 (1971).
19. Z. X. Mao and T. J. Hanratty, The use of scalar transport probes to measure wall shear stress in flow with imposed oscillations, *Exp. Fluids* **3**, 129 (1985).
20. A. Ambari, C. Deslouis and B. Tribollet, Frequency response of the mass transfer rate in a modulated flow at electrochemical probes, *Int. J. Heat Mass Transfer* **29**(1), 33 (1986).
21. N. Brauner, Roll wave celerity and average film thickness in turbulent wavy film flow, *Chem. Engng Sci.* **42**(2), 265 (1987).
22. N. Brauner, D. Moalem-Maron and W. Zijl, Interfacial collocation equations of thin liquid films in the presence of interfacial shear: stability analysis, *Chem. Engng Sci.* **44**(11), 2711 (1989).
23. N. Brauner, Frequency response of wall transfer probes to progressive waves, Report Faculty of Engineering, Tel-Aviv University, Israel (1989).

REPONSE EN FREQUENCES DES SONDES DE TRANSFERT A LA PAROI

Résumé—La réponse temporelle des sondes de transfert en paroi peut affecter de façon sensible l'interprétation des phénomènes physiques. La fonction de transfert entre le flux de chaleur ou de masse à la surface et le gradient de vitesse à la paroi est analysée dans le domaine de fréquence. Une variation spatiale induite par la vitesse finie de propagation d'une tension de cisaillement pariétale est considérée, comme cela peut être rencontré fréquemment dans des systèmes d'écoulement diphasiques. L'analyse indique que la réponse est déterminée par deux paramètres, la fréquence adimensionnelle et la vitesse adimensionnelle de fluctuation. Les corrections d'amplitude et de phase qui doivent être appliquées à des calculs de modèle pseudostatique sont calculées. On trouve que la réponse en fréquence se détériore significativement lorsque la fluctuation en paroi diminue. La sensibilité de la réponse à la fluctuation de vitesse diminue quand le nombre de Prandtl ou de Schmidt augmente, ce qui indique une supériorité des sondes électrochimiques sur les sondes thermiques.

ÜBER DEN FREQUENZGANG VON SENSOREN FÜR DEN WÄRME- UND STOFFTRANSPORT AN DER WAND

Zusammenfassung—Das Zeitverhalten von Sensoren für den Wärme- oder Stofftransport an der Wand kann die Interpretation der beteiligten physikalischen Phänomene wesentlich beeinflussen. Die Übertragungsfunktion zwischen der Wärmestrom- oder Massenstromdichte an der Oberfläche des Sensors und der Schubspannung an der Wand wird im Frequenzbereich analysiert. Räumliche Veränderungen werden berücksichtigt, die durch die endliche Ausbreitungsgeschwindigkeit einer fluktuierenden Wandschubspannung hervorgerufen und häufig in verschiedenen Zweiphasenströmungs-Systemen angetroffen werden. Die Untersuchung zeigt, daß die Antwort durch zwei Parameter bestimmt wird—die dimensionslose Frequenz und die dimensionslose Ausbreitungsgeschwindigkeit. Die Amplituden- und Phasenkorrekturen, die bei pseudostationären Modellrechnungen angewandt werden müssen, werden numerisch berechnet. Es zeigt sich, daß der Frequenzgang des Sensors bei einem Abnehmen der Fluktuation der Wandschubspannung wesentlich schlechter wird. Die Empfindlichkeit der Antwort gegenüber der Fluktuationsgeschwindigkeit wird geringer, wenn die Prandtl- oder die Schmidt-Zahl steigt. Dies zeigt eine Überlegenheit elektro-chemischer Sensoren gegenüber thermischen.

ЧАСТОТНАЯ ХАРАКТЕРИСТИКА ЗОНДОВ ДЛЯ ИЗМЕРЕНИЯ ПЕРЕНОСА НА СТЕНКЕ

Аннотация—Временная характеристика зондов для измерения переноса на стенке может существенно влиять на интерпретацию рассматриваемых физических явлений. В частотной области анализируется связь между плотностью теплового или массового потока на поверхности зонда и сдвигом на стенке. Исследуется пространственное изменение, вызванное конечной скоростью распространения флуктуирующего сдвига на стенке, что часто имеет место в различных системах двухфазных течений. Анализ показывает, что частотная характеристика определяется двумя параметрами: безразмерной частотой и безразмерной скоростью флуктуации. Численно рассчитываются поправки на ампилитудные и фазовые искажения, которые следует применять при численных расчетах на основе квазистационарных моделей. Найдено, что со снижением скорости флуктуаций сдвига на стенке частотная характеристика зонда значительно ухудшается. Чувствительность частотной характеристики к скорости флуктуаций уменьшается с ростом чисел Прандтля или Шмидта, что свидетельствует о преимуществе электрохимического зондирования перед тепловым.